

Nuclear electric-quadrupole interaction of ion-implanted ^{203}Hg and ^{69m}Zn in graphite

B. Kastelein, M. W. J. Prins, J. Andriessen, H. Postma, and L. Klostermann*

Delft University of Technology, Department of Applied Physics, P.O. Box 4056, 2600 GA Delft, The Netherlands

P. Herzog and J. Prinz

Institut für Strahlen und Kernphysik der Universität Bonn, Nussallee 14-16, D 5300 Bonn 1, Germany

(Received 29 January 1992)

^{203}Hg and ^{69m}Zn ions have been implanted into thin foils of highly oriented pyrolytic graphite at room temperature and at temperatures below 1 K. Low-temperature nuclear orientation due to strong electric-quadrupole interaction has been observed and the derived electric-field gradients are compared with two kinds of theoretical calculation. The first is based on the induced polarization of the graphite atoms, while in the second the hybridization of impurity and graphite electron wave functions is calculated. The results indicate that the fraction of nuclei that contribute to the macroscopic alignment is located in the layers of the C atoms. The experimental value of V_{zz} at the nuclear site of Hg is $+ [8.2(9)] \times 10^{22} \text{ V/m}^2$, parallel to the graphite c axis.

I. INTRODUCTION

The measurement of nuclear electric-quadrupole interaction (QI) provides information about the nuclear system of interest as well as the solid-state environment of the nucleus. In this sense, the system of impurity ions in graphite is of great interest, because the strongly noncubic structure of the graphite lattice may cause on the nuclear site of the impurity a large electric-field gradient (EFG) that interacts with the nuclear electric-quadrupole moment Q . Alignment of the spins of nuclei with respect to the principal axes of the EFG is obtained when the thermal energy is small compared to the quadrupole interaction energy and, consequently, in the case of radioactive nuclei, the angular distribution of the emitted γ rays will then become anisotropic. When this anisotropy is measured as a function of temperature in a low-temperature nuclear orientation (LT-NO) experiment, information on the hyperfine interaction can be extracted. In particular, the nuclear electric-quadrupole moment of the impurity is known, values for the EFG may then be obtained. Comparing this EFG with theoretical results for different lattice sites, a better understanding of the lattice location of the implanted impurity in graphite and of possible lattice formations may be gained. Alternatively, measuring the anisotropy effect of a pair of isotopes implanted under the same conditions gives a value for the ratio of the quadrupole moments (without the need for the knowledge of lattice locations and deformations).

Basically, there are two different ways of introducing impurities into the graphite lattice: ion implantation and intercalation. Ion implantation is a physical method applicable to nearly all elements. Intercalation is a chemical method, generally only possible for compounds. The advantage of ion implantation is that pure elements can be introduced into the lattice, while a disadvantage is the accompanying lattice damage, and consequently the final lattice location of the ion-implanted impurity cannot be determined.

In order to test the behavior of graphite as a host material for nuclear orientation and to study the QI, radioactive nuclei with known quadrupole moments have been intercalated or implanted in highly oriented pyrolytic graphite (HOPG). Other papers also report the detection of QI of ions as parts of compounds in graphite. All known experiments are summarized in Table I.

In this paper LT-NO measurements on ion-implanted Hg and Zn in thin foils of HOPG are reported, together with first-principles calculations of the EFG. HOPG is selected for nuclear-orientation studies because of its well-defined c axis. The hyperfine interaction is exclusively electric because graphite is a nonmagnetic solid and the implanted Hg and Zn ions have all their inner electronic shells closed.

For the LT-NO experiment, ^{203}Hg nuclei were implanted at room temperature. To test if the HOPG may be useful for on-line NO experiments—for measuring quadrupole moments of nuclei with half-lives shorter than, say, one hour—two low-temperature implantations were carried out. Thin foils of HOPG were kept at temperatures below 1 K while implanting respectively ^{203}Hg and ^{69m}Zn nuclei. In order to study the behavior of fractions of nuclei at different sites, LT-NO experiments were performed immediately after the implantation as well as after room-temperature annealing.

Apart from the measurements on ion-implanted Hg and Zn a theoretical investigation is made of possible locations. Further, theoretical calculations are performed to determine the EFG at the nuclear site of the impurities. Hg and Zn have the same atomic valence shell occupations ($5p^6 5d^{10} 6s^2$ and $3p^6 3d^{10} 4s^2$, respectively) and hence they are expected to show a similar electronic behavior in the same lattice locations. Theoretical calculations of the EFG are performed on the basis of a model of a free impurity ion embedded inside the graphite lattice as well as on the basis of a model in which the electronic wave functions of the impurity ion and of the carbon atoms hybridize.

TABLE I. Overview of QI of implanted and intercalated impurities in graphite.

Isotope	Implanted Technique	Ref.	Molecule	Intercalated Technique	Ref.
¹² B	NMR	1	¹¹¹ InCl ₃	TDPAC	2-4
¹⁹ F	TDPAC	5	¹³³ Cs ^c	Mössbauer	6
⁵⁷ Co	Mössbauer	7	¹⁸¹ HfCl ₄	TDPAC	8,9
^{69m} Zn	LT-NO	a	¹⁸² TaCl ₅	LT-NO	10
¹¹¹ In	LT-NO/TDPAC	44	²⁰³ HgCl ₂	LT-NO	b
¹³³ Xe	Mössbauer	11	¹²¹ SbF ₅	Mössbauer	12
¹⁶⁰ Tb	LT-NO	13	¹⁵² Eu ^c	Mössbauer	14
¹⁸¹ Hf	TDPAC	b			
¹⁸³ Re	LT-NO	b			
¹⁸⁸ Ir	LT-NO	15,43			
¹⁸⁹ Ir	LT-NO	43			
²⁰³ Hg	LT-NO	a			

^aPresent work.

^bUnpublished.

^c V_{zz} mainly originates from intercalate neighbors.

The remainder of the paper is organized as follows. First, experimental details are given. The formulas for γ -ray anisotropy in the particular case of oriented nuclei in HOPG will be introduced in Sec. III. Impurity lattice locations are proposed in Sec. IV together with the presentation of the theoretical calculations. The results and conclusions are given in the last two sections.

II. LT-NO EXPERIMENTS WITH HOPG

The crystalline structure of graphite consists of layers of hexagonally ordered *C* atoms in the well-known *ABAB* . . . stacking.¹⁶ The *c* axis is perpendicular to the layers that are separated by a distance $\frac{1}{2}c = 3.35$ Å; the distance between two atoms in the (*a*, *b*) plane is 1.42 Å (lattice constant $a = 2.46$ Å). The density of *C* atoms is $n = 8/(\sqrt{3}a^2c) = 1.14 \times 10^{29}$ m⁻³. The valence band structure consists of σ bands resulting from hybridized atomic *2s* and *2p_{x,y}* orbitals and of π bands from atomic *2p_z* orbitals parallel to the *c* axis. The former accounts for the strong bonding within the layers, while the latter is responsible for the weak van der Waals forces between the layers.

The conduction band (composed of antibonding σ^* and π^* bands) is only weakly occupied (10^{24} electrons/m³). This is the reason why graphite is called a semimetal. The density of states at the Fermi energy is 1.2×10^{-4} states/eV per *C* atom, a factor 10^2 – 10^3 less than for metals.¹⁷

HOPG is a synthetic form of graphite. It is composed of microcrystallites with dimensions of order of a few μ m, randomly oriented in the *a* and *b* directions, but well ordered in the *c* direction.¹⁸ The directional distribution of the *c* axes (mosaic spread) is less than 0.5° .¹⁹

The noncubic structure of graphite gives, at certain lattice sites, rise to very large EFG's interacting with the nuclear quadrupole moment of the impurity. At temperatures well below 1 K, when the QI is larger than the thermal energy, the nuclear electric-quadrupole moments

become aligned and the γ radiation of the radioactive nuclei may no longer be emitted isotropically. The γ -ray anisotropy depends on the decay properties and on the direction of emission with respect to the orientation axis. The electric QI can thus be observed by measuring the relative intensity change or anisotropy of γ radiation from the oriented nuclei as a function of temperature.

The decay scheme of ²⁰³Hg (half-life 46.6 days, nuclear spin $\frac{5}{2}$) is very simple: its β^- decay, $\frac{5}{2}^- \rightarrow \frac{3}{2}^+$ with $\log_{10}ft = 6.5$, is followed by a γ -ray transition of 279 keV to the $\frac{1}{2}^+$ ground state of ²⁰³Tl. Assuming that the β^- -transition carries away only one unit of angular momentum, the second-order anisotropy parameter (see Sec. III) of this mixed transition with $\delta(E2/M1) = +1.17(5)$ (Ref. 20) is calculated to be $A_2U_2 = -0.6984(16)$, while in this case by definition $A_4U_4 = 0$. The uncertainty in A_2U_2 is due to the uncertainty in δ . The mentioned sign of A_2U_2 (which depends on the sign of δ) agrees with the observed anisotropies²¹ of ²⁰³HgFe. The value for the nuclear electric-quadrupole moment $Q = +0.343(36)$ b.^{22,23}

^{69m}Zn (half life 13.8 h, nuclear spin $\frac{9}{2}$) decays by internal *M4* transition directly to the stable ground state, emitting a 439-keV γ ray. The anisotropy parameters are $A_2U_2 = -0.9358$ and $A_4U_4 = +0.5322$ and $Q = -0.51(5)$ b.²³ Higher-order terms can be neglected for the purposes of this paper.

III. γ -RAY ANISOTROPY IN HOPG

The general expression for the normalized intensity of γ rays measured from an oriented ensemble in a direction specified by polar angles (θ, ϕ) in the laboratory frame is²⁴

$$W(\theta, \phi) = \sqrt{4\pi} \sum_{\lambda, q} \left(\frac{2I+1}{2\lambda+1} \right)^{1/2} A_\lambda U_\lambda Q_\lambda \rho_q^\lambda(I) Y_{\lambda q}^*(\theta, \phi). \quad (1)$$

The statistical tensors $\rho_q^\lambda(I)$ describe the oriented state

from which the radiation is emitted, and I is the nuclear spin. The A_λ coefficients describe the properties of the emitted radiation, the U_λ are known as deorientation coefficients and depend on properties of preceding transitions, and the Q_λ correct for the finite solid angle of the γ -ray detector. The $Y_{\lambda q}(\theta, \phi)$ are spherical harmonics, with $0 \leq \lambda \leq \min(2I, 2L)$ and λ even, while $-\lambda \leq q \leq \lambda$ (L being the multipolarity of the γ transition). The statistical tensors contain information on the QI and depend on the temperature. They can be calculated following a procedure that involves calculating the energy eigenvalues and eigenstates of the Hamiltonian and the density matrix of the ensemble.^{24,25}

In the particular case of HOPG there are two important details: (i) Averaged statistical tensors are needed because of the microcrystallites, and (ii) various lattice locations give rise to different anisotropy functions, which must be summed with proper weight factors.

Because of the random orientation of the microcrystallites in HOPG in the (a, b) plane, averaged statistical tensors²⁶ must be calculated. This calculation involves two frames of reference: S_C and S_H . The z axis of frame S_C is parallel to the graphite c axis, while S_H is the frame of the Hamiltonian of the orienting system, e.g., a nonaxial QI :

$$\mathcal{H} = P \left[I_z^2 - \frac{1}{3} I(I+1) + \frac{1}{6} \eta (I_+^2 + I_-^2) \right]. \quad (2)$$

In Eq. (2) $P = 3eQV_{zz}/4I(2I-1)$ is the strength of the nuclear electric QI (often expressed as a frequency of $\nu_Q = eQV_{zz}/h$), V_{zz} is the electric-field gradient along the quantization direction, and η is the asymmetry parameter [$\eta = (V_{xx} - V_{yy})/V_{zz}$; $0 \leq \eta \leq 1$]. In this description, S_H is the principal-axes system of the EFG tensor at the nuclear site, with the usual convention $|V_{zz}| \geq |V_{yy}| \geq |V_{xx}|$.^{27,28}

The transformation of the spherical tensors in frame S_H to spherical tensors in frame S_C is performed with the aid of rotation matrices. In Fig. 1, examples are given for the charge distribution of nonaxial EFG's with orientations of S_H that will be used in Sec. IV B. Because of the distribution of microcrystallites an averaging is required over all orientations of frame S_C in the graphite lattice

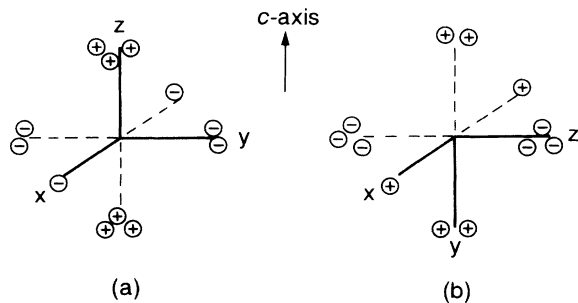


FIG. 1. Two different directional orientations of S_H with respect to S_C . The number of + or - signs simulates the value of the EFG component along the corresponding axis of S_H . Only the z axis (or c axis) of S_C is drawn (a) $V_{zz} > 0$, $\eta \neq 0$, $\beta = 0$, $\alpha = 0$, (b) $V_{zz} < 0$, $\eta \neq 0$, $\beta = \pi/2$, $\alpha = -\pi/2$.

and so only statistical tensors $\rho_0^\lambda(S_C)$ are observable. Note that they still contain contributions of $\rho_{q \neq 0}^\lambda(S_H)$ of the local nonaxial QI :

$$\rho_0^\lambda(S_C) = \left(\frac{4\pi}{2\lambda+1} \right)^{1/2} \sum_q Y_{\lambda q}(\beta, \alpha) \rho_q^\lambda(S_H). \quad (3)$$

Here, α, β are the Eulerian angles for rotating the frames of S_H (which are randomly oriented in the plane perpendicular to the c axis) to frame S_C : α around the z axis of S_H and β around the new y axis. See the two examples of Fig. 1.

Besides the presence of microcrystallites, different lattice locations can play a role in the observable spherical tensors. If the ions occupy various lattice locations in graphite, a weighted sum of anisotropy functions will be observed. In this paper a fraction model is used for a fit to the experimental results. In this model the impurity ions are supposed to occupy a number of different lattice sites with their own EFG. Nuclei in lattice sites with randomly oriented EFG's do not contribute to the macroscopic nuclear orientation and are represented by a nonorienting fraction. The measured statistical tensor is written as $\rho_0^\lambda(S_C) = \sum_i f_i \rho_0^\lambda(S_C)$, where the fractions f_i and the nonorienting fraction add up to unity.

Summarizing, the anisotropy of γ rays emitted from radioactive nuclei in HOPG can be calculated as a function of (a) the magnitude of the various fractions f_i^* , (b) for each fraction, the magnitude and direction of the nuclear electric QI (P, η, α , and β); and (c) the absolute temperature, T .

IV. THEORY

A. Possible lattice locations

When atoms are implanted in graphite the absorption of kinetic energy causes lattice damage along the implantation track. This damage includes the creation of vacancies near the final position of the implanted atom. Therefore in graphite implanted atoms are supposed to occupy lattice locations *inside* the layers as well as lattice locations *between* layers. As indicated in Fig. 2, in this paper the following relatively simple impurity configurations

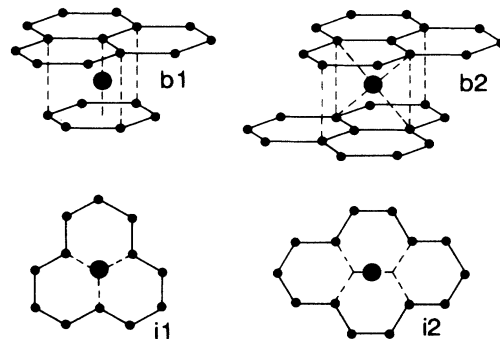


FIG. 2. Lattice locations considered in this paper. The impurity ion is represented by a thick dot. The solid lines indicate σ bonds between the carbon atoms.

will be considered: b1, between the layers, with point group C_{3v} ; b2, between the layers, with point group C_{2h} ; i1, in the layers, with point group D_{3h} ; i2, in the layers, with point group D_{2h} .

The indicated symmetry groups apply to the local environment of the impurity ion as given in Fig. 2. Lattice locations b1 and i1 have a threefold symmetry axis parallel to the c axis; lattice locations b2 and i2 have a twofold symmetry axis perpendicular to the c axis. In lattice location b1 inversion symmetry is absent, because the ion is being held between a single C atom on one side and a ring of C atoms on the other side. Therefore, the ion will not be situated exactly in the middle of the two layers, but will be displaced in the direction of the ring of C atoms.

The available space in the graphite lattice and the bonding possibilities determine the probability of the various lattice locations. The location of an atom or ion will depend on the combined bonding and repulsion energy. The repulsion energy was estimated on the basis of a repulsion potential $\propto r^{-m}$. Taking $m=12$ (Lennard-Jones potential) or $m=8$ (like in ionic crystals²⁹) and taking the lattice constants of Sec. II, it appears that lattice locations b1, b2, and i2, which offer approximately the same space, have roughly the same repulsion energy and that the substitutional lattice location i1 has a repulsion energy that it at least give times larger than the other three impurity configurations. Concerning location i2, Kaxiras and Pandey³⁰ performed calculations with a C atom in the location i2. The four nearest neighbors move towards the central C atom, forming four weak bonds to it. Thus, in lattice location i2 weak bonding may also be the case for impurity atoms other than carbon, provided that their radius is not larger than 1 Å approximately.

In total, this leads to the conclusion that lattice location i1 is only probable for small impurities that strongly hybridize with the graphite lattice, boron being an example.¹ For larger atoms like Hg and Zn, lattice locations b1, b2, and i2 are more realistic.

B. Calculation of the EFG

Two different methods were used for calculating the EFG at the impurity site: (i) the simple and classical approach of considering the implanted ion as a free ion, i.e., neglecting the overlap of the electronic charge densities of the implanted ion and the graphite atoms and (ii) the quantum-mechanical approach taking into account the hybridization of all electronic orbitals. The former will provide some insight into the mechanism causing the

EFG, but gives no accurate values; the latter, when applied to the calculation of an EFG on impurities in graphite, is expected to be more rigorous.

1. Free-ion model

In a free-ion model the EFG is caused by the electric multipoles of the atoms surrounding the impurity, and is enhanced by the electronic cloud of the impurity itself. This enhancement is described with the factor $(1-\gamma_\infty)$; for Zn^{2+} and Hg^{2+} the Sternheimer antishielding factors are $\gamma_\infty = -12.31$ and -60.20 , respectively.³¹ The multipoles surrounding the impurity can for example be point charges in the case of an ionic host crystal. They can also be *induced* by the ionic charge of the impurity itself.

In the case of graphite one expects the impurity metal to acquire a positive ionic charge. Campbell *et al.*⁶ have suggested the attraction of shielding conduction electrons around the impurity ion as one of the mechanisms causing an EFG. But this effect is unlikely to be of importance, since the density of states at the Fermi-level $\mathcal{D}(\epsilon_F)$ of graphite is very small. One may notice that the Thomas-Fermi wavelength of screening, $2\pi/k_s$, is larger than 100 Å in graphite. The wavelength of screening is calculated with the relation²⁹ $k_s^2 = (e^2/\epsilon_0) \mathcal{D}(\epsilon_F) n$, with the values for $\mathcal{D}(\epsilon_F)$ and the density of C atoms n as given in Sec. II. On the other hand, the ionic charge of the impurity can induce electric dipoles on its surrounding carbon atoms. In order to calculate the EFG due to this lattice polarization, all carbon atoms were considered as point dipoles obeying $\mathbf{p} = \alpha_p \cdot \mathbf{E}$. Here, \mathbf{p} is the atomic dipole moment of the C atom, α_p is its isotropic polarizability, and \mathbf{E} is the electric field at the lattice site. This electric field results from the point charge q of the ion and from the other dipoles in the graphite lattice. An estimation of α_p can be obtained through calculations on a free C^{2+} atom,³² or through calculations on the transverse polarizability of σ bonds in diamond.³³ The first gives $\alpha_p = 0.67 \times 10^{-24} \text{ esu} = 7.5 \times 10^{-41} \text{ C m}^2/\text{V}$, the second gives $\alpha_p = 3.27 \text{ a.u.} = 5.4 \times 10^{-41} \text{ C m}^2/\text{V}$.

At several lattice locations in graphite the self-consistent lattice polarization has been calculated with an iterative computer program. The resultant EFG on the ion is given in Table II, taking the lattice constants of pure graphite and using the lower value of $\alpha_p = 5 \times 10^{-41} \text{ C m}^2/\text{V}$; larger values of α_p caused instabilities in the lattice sum calculation. Lattice locations b1, b2, and i2

TABLE II. EFG in a free-ion model due to lattice polarization. The graphite lattice was undisturbed, the polarizability of the C atom was $\alpha_p = 5 \times 10^{-41} \text{ C m}^2/\text{V}$. In lattice location b1 the ion was off centered with 5% of lattice constant c . V_{zz} is in units of 10^{22} V/m^2 and is calculated taking $q=2$ and the Sternheimer parameters as mentioned in the text.

Position	V_{zz} (10^{22} V/m^2)	η	β (deg)	α (deg)	$V_{zz}(Zn^{2+})$ (10^{22} V/m^2)	$V_{zz}(Hg^{2+})$ (10^{22} V/m^2)
b1	-0.017 q	0.0	0.0	0.0	-0.43	-2.0
b2	-0.023 q	0.14	12.5	-90	-0.58	-2.8
i1	+0.075 q	0.0	0.0	0.0	+1.9	+9.2
i2	+0.020 q	0.23	0.0	0.0	+0.50	+2.4

yield an EFG at the ion of approximately the same absolute value. Taking $q=2+$ as the maximum ionic charge of Hg and Zn in graphite, and using the Sternheimer parameters mentioned above, the free-ion point-polarization model gives a V_{zz} at the nuclear site with an absolute value of about 2.5×10^{22} V/m² for Hg and about 0.50×10^{22} V/m² for Zn; V_{zz} has a negative sign for lattice locations between the graphite layers and a positive sign for lattice location i2 inside the layers. In all lattice locations except b2, the z axis of the EFG is parallel to the c axis of graphite (Euler angle $\beta=0$). In lattice location b2 the Euler angles are $\beta=12.5^\circ$ and $\alpha=-90^\circ$ (x axis of the EFG perpendicular to the c axis). The angle 12.5° is understandable from the geometry of this position, see Fig. 2.

2. Hybridization model

First-principles calculations were carried out for the EFG of Hg and Zn in the above mentioned impurity centers in graphite, using the GAUSSIAN 90 system of programs,³⁴ released by the Carnegie Mellon University in Pittsburgh, PA. With this computer program, all electronic interactions in a predefined cluster are calculated. The carbon lattice including the impurity was modeled as a relatively small cluster of atoms of which the dangling bonds were closed by hydrogen atoms.³⁵ The molecular wave function (from which the EFG can be derived) is constructed from a linear combination of atomic orbitals (LCAO) using a variational technique. The atomic orbitals, forming the basis set, are each in the form of a sum of Gaussian functions.

The clusters are schematically drawn in Fig. 2 and the calculations were done for Zn and Hg in the positions i1, i2, and b1.

Tables of Huzinaga³⁶ were used for the atomic basis sets of Zn and Hg. For carbon and hydrogen Slater-type orbitals approximated by a sum of three Gaussians (STO-3G) bases were used. In order to have more freedom for the metal ions to adjust to the surroundings, additional valence p orbitals were added to the minimal basis: $4p$ for Zn and $6p$ for Hg. These were obtained from numerical wave functions fitted to the Gaussian form. Finally splitted core p orbitals were used: $3p$ for Zn and $5p$ for Hg,³⁷ in order to give the functions more freedom to hybridize.

The carbon-carbon distance in the layers was kept unchanged at 1.42 Å. It is not easy to get a realistic distance between the layers when an atom is implanted. In order to investigate the influence of this distance on the

EFG of an impurity in position b1, the distance was varied between 3.2 and 4.0 Å. It was found that the change of the EFG was less than 20% and so subsequent calculations were done for the "mean" value $d=3.6$ Å, which is slightly larger than the distance (3.35 Å) without impurities. The calculations also showed that the EFG at the in-layer positions i1 and i2 hardly depends on the presence of neighboring planes.

Important quantities are the EFG parameters V_{zz} and η at the nuclear site of the implanted ion and the orientation of the principal axes with respect to the crystallographic c axis (angles α, β), the overall charge q_{metal} of the implanted metal ion, and the sensitivity of the EFG parameters to the atomic basis sets.

The results for the positions i2 and b1 before and after adding valence orbitals to the impurity basis sets are listed in Table III. They show a remarkable difference in the values and composition of the EFG at the two hypothetical sites. At the in-layer position i2 the EFG comes out positive with a value of the asymmetry parameter η that depends on the basis set; the position b1 between the layers has a negative V_{zz} , the value of which depends very much on the presence of the valence orbitals.

For position i2 the dependence on these additional valence orbitals ($4p$ for Zn and $6p$ for Hg) is small. This is understandable from the expected low-lying carbon σ bonds in the in-layer direction. One may therefore expect the added metal valence orbitals to be relatively high in energy and thus not to be populated.

This is in great contrast with the results found for the other position b1 between the layers. The EFG is now the result of two strongly competing contributions, one being negative, arising from the core p orbital ($3p$ for Zn and $5p$ for Hg) and the other of positive sign, arising from the valence p orbitals. The resulting negative EFG will be small compared to the one in position i2. This was expected because the π orbitals of carbon perpendicular to the layers are high in energy. Thus they hybridize easily with the added metal valence orbitals, leading to a more spherical charge distribution. This picture is supported by the much smaller values of q_{metal} . When the nearest carbon atom in the neighboring graphite plane is removed, V_{zz} at Hg reduces to -2×10^{22} V/cm². Also, it was verified that V_{zz} changes sign smoothly when the Hg atom is moved from the between-layer position towards this vacancy, i.e., towards position i1.

Not shown in the table is the dependence of β on the overall charge of the cluster. In most cases, this charge was taken to be 0 or +1. In the Zn case, however, also a

TABLE III. Results of cluster calculations of Zn and Hg impurities in graphite at two hypothetical sites, calculated before and after adding valence orbitals. q_{metal} is in units of the elementary charge $|e|$ and V_{zz} is in units of 10^{22} V/m². In all cases, the principal z axis was parallel to the graphite c axis ($\beta=0$).

Impurity	$q_{\text{metal}} e $	Position i2		Position b1		η
		V_{zz} (10^{22} V/m ²)	η	V_{zz} (10^{12} V/m ²)	η	
Zn(4s) ^a	+1.25	+3.63	0.21	-10.4	0.0	0.0
Zn(4p)	-0.11	+3.47	0.04	-1.52	0.0	0.0
Hg(6s)	+1.56	+15.5	0.29	-6.76	0.0	0.0
Hg(6p)	+0.40	+14.5	0.13	-4.14	0.0	0.0

^aWith cluster charge $+2e$: $V_{zz} = -3.8 \times 10^{22}$ V/m², $\eta=0.15$, $\beta=90^\circ$, and $\alpha=-90^\circ$.

charge of +2 was taken, but without the presence of the additional valence p shell. Now the angle β came out to be 90° with $V_{zz} < 0$ and $\alpha < 0$. Therefore, it remains possible that with a certain choice of the basis set and total cluster charge the EFG is oriented perpendicular to the c axis [as in Fig. 1(b)]; the component parallel to the c axis remains positive. The change of principal axes is the result of changing the occupation of p_x - and p_y -type molecular orbitals.

Concerning position i1, only solutions for Zn were obtained with an increased carbon-carbon distance of 1.60 Å, indicating that for this position the lattice must be distorted. This is in agreement with the repulsion energy calculations of Sec. IV A. The results were $V_{zz} = +6.1 \times 10^{18}$ V/cm², $\eta = 0$, $\beta = 0$. The positive value of V_{zz} is in agreement with the results for boron in this substitutional position.¹

3. Comparing the models

Two models have been proposed and applied for explaining the measured EFG of implanted ions in graphite. The EFG is very likely not the result of the conduction electrons but of polarization of the graphite charge cloud. Shielding effects are not easy to estimate in the free-ion model; they are expected to be small and are therefore neglected. The charge of the implanted ions is thus set to the maximum value corresponding to an empty valence shell. The values of the EFG in the free-ion model come out roughly three times smaller than the experimental results described in the next section. The hybridization model gives an EFG which is around two times too high, but also gives information about the existence of impurity levels and shielding effects. The results are preliminary because in certain lattice locations there is much dependence on the basis set. However, both models convincingly agree on the following results.

In position b1, $V_{zz} < 0$ parallel to the c axis and $\eta = 0$. In positions i1 and i2, $V_{zz} > 0$ parallel to the c axis and $\eta = 0$ (position i1) or η is small (position i2); position i1 is energetically unfavorable. The principal x axis is perpendicular to the c axis in all positions (i.e., $\alpha = -\pi/2$).

In addition, the hybridization model shows that, in position i2, the following is also possible: For $V_{zz} < 0$ perpendicular to the c axis and $\eta \neq 0$, the EFG between the layers is expected to be small, because of the two contributions that are of opposite sign.

Because of the important qualitative agreement of the two models, it can be concluded that lattice polarization gives a fair description of the origin of the EFG in graphite. However, when more precise EFG's are needed, the overlap of electron wave functions must be considered.

4. Experimental fitting

In an LT-NO experiment, only nuclei that experience a large QI with the same direction of orientation will contribute to the γ -ray anisotropy. In the picture outlined above, this corresponds to the fraction of nuclei that ends up *inside* the layers. The other fractions are thought to be located between the layers with much smaller EFG's

or are randomly oriented due to implantation damage. The experimental data are analyzed according to the following parameter-models.

(1) One orienting fraction with axially symmetric QI with principal z axis of the EFG parallel to the c axis ($\beta = 0$, $\eta = 0$). The fraction f and the interaction strength P are free parameters.

(2) One orienting fraction with non-axially-symmetric QI with principal x and z axes of the EFG perpendicular to the c axis ($\alpha = -\pi/2$, $\beta = \pi/2$). The parameters are f , P , and η .

(3) Two orienting fractions with axially symmetric QI with respect to the c axis; one fraction with V_{zz} positive—representing nuclei inside the layers—and one with V_{zz} negative—representing nuclei between the layers—($\beta^{1,2} = 0$, $\eta^{1,2} = 0$). The parameters are $f^{1,2}$ and $P^{1,2}$.

When the nuclei between the layers experience a small $|V_{zz}|$, as is calculated in the hybridization model, parameter model 3 approaches parameter model 1.

These parameter models were fitted to the LT-NO data (with the CERN minimization routine MINUIT) and results for the parameters are presented in Sec. VI.

V. EXPERIMENTAL DETAILS

HOPG foils with thickness of about 30 μm and area of 12×12 mm² were peeled off from a thick piece of HOPG using Scotch tape. Afterwards, the tape was removed by dissolving it in acetone. ²⁰³Hg was implanted into the surface of the graphite foil, opposite to the side where the Scotch tape had been attached. In the ^{69m}Zn experiment a foil of thickness of 90 μm was cleaved from the bulk with a sharp razor blade. In this way, no Scotch tape was used and both sides of the foil had clean surfaces.

The room-temperature implantation of ²⁰³Hg was performed using the ISOLDE-3 isotope separator at CERN with ion currents of about 8.0 pA; an activity of 20 kBq of ²⁰³Hg was collected in the graphite foil. From the activity and implantation area an implantation dose of 3.1×10^{11} atoms/cm² was calculated; the amount of other isotopes implanted can be neglected. The implantation energy was 60 keV. The LT-NO experiment was carried out at Delft, where the implanted foil was clamped between two copper plates and mounted onto the mixing chamber of a dilution refrigerator equipped with a PrNi₅ demagnetization stage. The anisotropy was measured at various temperatures between 100 and 4.5 mK. Temperatures were determined with a ⁶⁰CoCo(hcp) nuclear orientation thermometer below 35 mK and with Germanium resistance thermometry above 50 mK. When the demagnetization stage is used, the magnetic field at the site of the sample was less than 0.5 mT due to compensation coils. The γ rays of ²⁰³Hg and ⁶⁰Co were detected with a 3" \times 3" NaI(Tl) detector placed parallel to the graphite c axes and with a Ge(Li) detector perpendicular to it. Because of the low activity of ²⁰³Hg, anisotropies could only be observed with the more efficient NaI(Tl) detector.

Before the cold implantation of ²⁰³Hg in Bonn, a foil of HOPG was soldered with eutectic GaIn and simultane-

ously clamped with a copper plate (with a hole in the center for the implantation) onto the cold finger of the dilution refrigerator, together with a $^{54}\text{MnNi}$ nuclear orientation thermometer. The refrigerator was cooled to the lowest-temperature region before the ^{203}Hg implantation started. During implantation, the temperature was kept below 0.2 K. At these temperatures annealing effects do not occur. The implantation energy was 80 keV, the implantation dose was estimated to be less than 2×10^{14} atoms/cm 2 and the implanted activity was about 19 kBq. In order to magnetically saturate the nickel foil of the ^{54}Mn thermometer and to prevent the GaIn from getting superconductive, an external magnetic field of 0.54 T was applied perpendicular to the graphite c axis.

Directly after the implantation, the sample was cooled to low temperatures and the anisotropy in the directional distribution of the γ rays was measured both parallel and perpendicular to the c axis as a function of temperature using Ge(Li) detectors. After this experiment, the sample was annealed at room temperature, cooled down again to 7.0 mK and the measurements were repeated.

The ^{69m}Zn experiment was completely analogous, but now with an estimated implantation dose $< 1 \times 10^{14}$ atoms/cm 2 . The implanted activity was about 52 kBq and the anisotropies were measured at 8.1 mK before and at 7.7 mK after room-temperature annealing. Because of the short half-life and the low activity it was not sensible to measure the ^{69m}Zn γ anisotropy at several different temperatures.

VI. RESULTS AND DISCUSSION

A. Implantations of ^{203}Hg

In Fig. 3 plots are presented of the γ -ray anisotropies of the 279-keV transition of implanted ^{203}Hg measured at various temperatures. Experiment (a) is done after room-temperature implantation, experiment (b) directly after cold implantation, and experiment (c) after annealing the cold implanted sample at room temperature. The solid lines represent least-squares fits on the basis of model 1 described above. A large γ -ray anisotropy occurs after the warm implantation, while the cold implanted sample only shows considerably anisotropy after annealing. The linear behavior of the anisotropy at low values of the inverse temperature is typical for pure electric QI. The departure from the linear behavior at $T = 10$ mK (not often seen in QI experiments) reveals the strength of the QI.

In Table IV the results are given of fits on the basis of the three parameter models, together with the reduced χ^2 in order to discriminate between them. From the QI constant P values for V_{zz} are calculated, which are also presented in the table; note that the uncertainty in Q has a large effect on the uncertainty in V_{zz} . Because of the large errors, experiment (b) is not used in parameter models 2 and 3.

In parameter model 1, the values for P agree well within one standard deviation for the three *independent* experiments. The QI is very strong, but the measured anisotropy is reduced because only a small fraction of orienting nuclei contributes. The cold implantation has a

negative influence in this respect. The different thermal treatments only influence the orienting fraction f . Weighting with $1/\sigma^2$, the average EFG is $V_{zz} = +[8.19(87)] \times 10^{22} \text{V/m}^2$. The influence of nonaxiality on the results for the EFG was established to be small.

In parameter model 2, the average is $V_{zz} = -[11.8(11)] \times 10^{22} \text{V/m}^2$; the negative sign agrees with the cluster calculations for position i2. It turns out that the data are not sensitive to η . Because in this model the principal z axis of the EFG lie in the (a, b) plane, smaller anisotropies in the direction parallel to the c axis occur and thus larger values are found for the fitted orienting fraction.

In parameter model 3, the result for V_{zz}^2 , the negative EFG, is unrealistically large in absolute value. The fraction of nuclei that experience this negative EFG (between

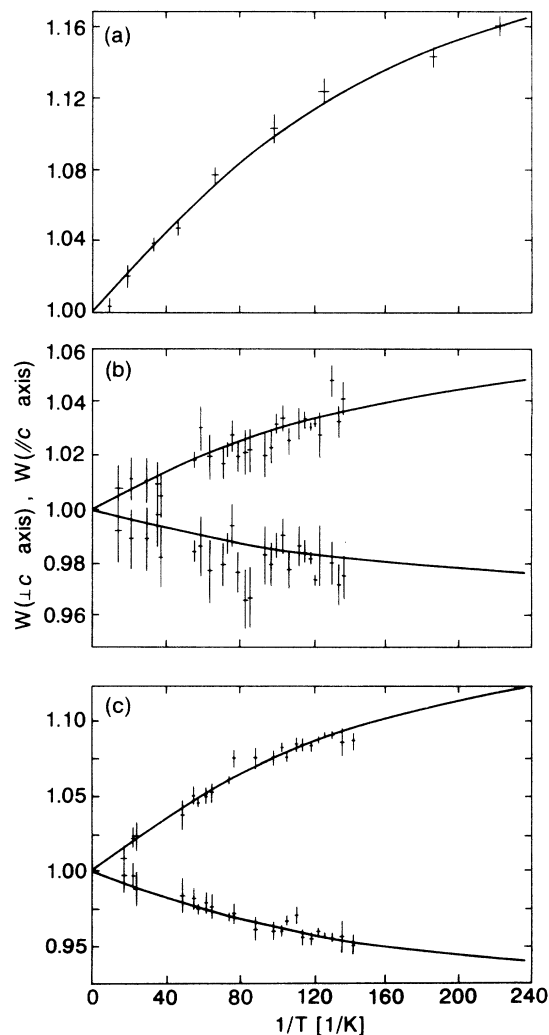


FIG. 3. The measured anisotropy of the 279-keV γ transition of ^{203}Hg as a function of the inverse temperature for (a) the room-temperature implanted sample, (b) the cold implanted sample, and (c) the room-temperature annealed cold implanted sample. Note that the scaling of the anisotropy axes in the plot is different for every measurement. The error bars indicate one standard deviation and the solid lines are least-squares fits on the basis of model 1.

TABLE IV. Results of fits on the data of experiments (a), (b), and (c) of ^{203}Hg on the basis of the three different models, with the corresponding values of the reduced χ^2 . The errors denote one standard deviation. From the fitted values of the QI constant P/k (in mK) and the known value of Q , the results for V_{xx} (in 10^{22} V/m 2) have been calculated. Because the parameters that can be deduced from experiment (b) have large errors, they are only given for model 1.

Expt	P/k	f	Parameter model 1		
			χ^2	V_{zz}	
<i>a</i>	+2.36(25)	0.352(23)	0.978	+7.9(12)	
<i>b</i>	+2.4(1.0)	0.085(27)	1.038	+7.9(3.5)	
<i>c</i>	+2.57(31)	0.211(18)	0.973	+8.6(1.4)	
Expt	P/k	η	Parameter model 2		
			f	χ^2	V_{zz}
<i>a</i>	-3.30(24)	0.00(65)	0.446(19)	1.202	-11.1(1.4)
<i>c</i>	-3.80(26)	0.00(75)	0.252(11)	0.974	-(12.7(1.6))
Expt	f^1	f^2	Parameter model 3		
			χ^2	V_{zz}^1	V_{zz}^2
<i>a</i>	0.400(12)	0.090(30)	1.274	+16.1(3.0)	-42.6(9.5)
<i>c</i>	0.290(3)	0.105(4)	0.974	+22.2(3.7)	-40.2(8.2)

the layers) does not seem to depend on the implantation conditions; annealing only improves the fraction with a positive EFG (in the layers). According to this model, after heat treatment more nuclei end up at in-layer positions after the heat treatment. The magnitude of the negative EFG is in contrast with the conclusions of the cluster calculations in position b1 that the EFG between the layers will be small and negative; parameter model 3 seems to be less useful for describing the results.

It is only possible to distinguish between the two remaining models after taking the theoretical results into account. In these calculations the possibility of V_{zz} being oriented perpendicular to the c axis comes out very unlikely and so parameter model 1 is taken to be the best candidate.

In Table V the measured V_{zz} of ^{203}Hg in graphite (following parameter model 1) is compared to the V_{zz} at isotopes of Hg implanted in several noncubic metal hosts. The V_{zz} in HOPG is almost an order of magnitude larger, demonstrating the significance of this material for measuring QI.

B. Implantation of ^{69m}Zn

The measured anisotropies of the 439-keV transition of the cold implanted Zn were $W(\parallel c)=0.983(2)$ and

TABLE V. LT-NO results for electric-field gradients at the nuclear site of Hg isotopes in different noncubic metals and in HOPG. The values are recalculated from the reported interaction frequencies with the more recent values of $Q(^{197m}\text{Hg})=+1.24(14)$ b and $Q(^{195m}\text{Hg})=+1.08(11)$ b of Ref. 22.

Experiment	V_{zz} (10^{22} V/m 2)	Reference
$^{197m}\text{HgZn}$	+1.60(19)	38
$^{197m}\text{HgCd}$	+1.43(19)	38
$^{195m}\text{HgCd}$	+2.13(36)	39
$^{197m}\text{HgRe}$	-0.367(65)	38
$^{197m}\text{HgSb}$	+0.233(35)	40
^{203}HgC	+8.19(87)	Model 1, this work

$W(\perp c)=1.017(2)$ at $T=8.1$ mK before, and $W(\parallel c)=0.982(3)$ and $W(\perp c)=1.011(3)$ at $T=7.7$ mK after annealing.

With this sample, annealing hardly improved the orienting fraction; only the ratio $W(0)/W(90)$, which is determined by the spherical harmonics of Eq. (1), improved. This annealing behavior is different from that of Hg and is not well understood, given the electronic similarities of Hg and Zn. The difference must be ascribed to the different ionic radii (0.74 Å for Zn^{2+} and 1.10 Å for Hg^{2+}) and different conditions during the ion implantation. Also, with the same implantation energy, the Zn ions have a larger velocity and therefore a larger implantation depth.

The sign of the γ -ray anisotropy is opposite to that of ^{203}Hg , as is expected from the signs of the respective quadrupole moments and A_2U_2 values. Because of the small number of data points, values for P can only be obtained for fixed values of f . If the orienting fraction lies between 25% and 8% [realistic values in view of experiments (b) and (c) on ^{203}Hg] then V_{zz} ranges from $+ [0.70(12)] \times 10^{22}$ to $+ [2.17(53)] \times 10^{22}$ V/m 2 with parameter model 1, and from $- [1.52(28)] \times 10^{22}$ to $- [6.3(1.6)] \times 10^{22}$ V/m 2 with parameter model 2.

C. Heat input and thermal gradients

Because of the rather poor heat conductance of graphite in the c direction at low temperatures, the heat input associated with the radioactive decay may give rise to thermal gradients inside the graphite lattice. The observed onset of saturation in the anisotropy of ^{203}Hg may then not be a real QI effect. The following arguments unambiguously show that the heat conductance cannot be a problem in these experiments and that the saturation in the anisotropy is indeed due to strong nuclear electric QI.

Estimates for the heat input, the implantation depth, and for the heat conductance coefficient λ_c are needed.

Under the assumption that all β particles and conversion electrons dissipate their kinetic energy homogeneously

ously into the whole graphite sample, the heat inputs from the decay of ^{203}Hg and ^{69m}Zn are 2.3×10^{-2} and 7.6×10^{-2} pW/Bq, respectively. With the thin samples of order of 10–100 mg/cm² the amount will actually be much less, since most of the heat is dissipated outside the graphite.

The implantation depth, or projected range R_p , and its fluctuation ΔR_p (between parentheses) can be estimated with the Lindhard, Scharff, and Schiott (LSS) theory:⁴¹ 200(32) Å, 260(40) Å, and 460(110) Å, for a 60-keV Hg, a 80-keV Hg and a 80-keV Zn ion colliding on graphite, respectively.

Values for λ_c are obtained from a separate experiment, where the heat conductance of HOPG foils with different thicknesses has been measured at temperature down to 20 mK.⁴² These samples were prepared in the same way and from the same material as the foils of this paper. Extrapolated values at $T=5$ mK are $\lambda_c = 2 \times 10^{-9}$ and 1×10^{-8} W/mK for a foil that was pulled with Scotch tape and for a foil that was cut with a razor blade, respectively.

With the above values the temperature profile in the graphite foil, which is cooled from two sides, can be calculated. The temperature gradient across the implanted layer, which only extends to at most 460 Å from the surface, is less than 0.1 mK at $T=5$ mK for the implanted activities of this paper. Because both copper and graphite are conductors, the thermal resistance across their contact is negligible.

As an additional argument against thermal saturation, the values for the QI constant P of ^{203}Hg in the three independent experiments agree well within one standard deviation, despite different heat inputs and mounting techniques.

VII CONCLUSIONS

The anisotropy data for ^{203}Hg and ^{69m}Zn implanted in HOPG reveal a strong nuclear electric QI and also a large nonorientating fraction of roughly 60%. Attempts to explain this large nonorienting fraction by assuming contributions of fractions with negative and positive EFG's (parameter model 3) have failed: The orienting fractions remain small and the fitted EFG's are found to be unrealistically large with large errors.

The theoretical calculations have provided a number of important details about the origin of the EFG in graphite. The EFG is very likely the result of polarization effects induced by the charge of the implanted ion, which is partly shielded. For both in-layer as well as between-layer positions V_{zz} is directed parallel to the graphite c axis. Under certain circumstances, in-layer positions may have V_{zz} oriented perpendicular to the c axis.

Two theoretical models, the free-ion model and the hybridization model (molecular cluster), are found to be useful for describing the origin of the EFG. The first model (no shielding) gives for Hg in the assumed in-layer position a value of $+2.4 \times 10^{22}$ V/m² compared to the experimental value of $+ [8.19(87)] \times 10^{22}$ V/m². The results of the cluster calculation is $+14.5 \times 10^{22}$ V/m², where the ionic charge changed from the free-ion value $+2$ to $+0.4$, a charge shielding of 80%. For Zn the experimental results are not very accurate and restrict V_{zz}

to the interval from $+0.70 \times 10^{22}$ to $+2.2 \times 10^{22}$ V/m². The theoretical results for the in-layer position are $+0.50$ for the free-ion model and $+3.5 \times 10^{22}$ V/m² for the cluster calculation, where the charge ascribed to the Zn ion was -0.11 ion, which has to be compared with the free-ion value $+2$.

For the between-layer position of the V_{zz} is negative (for both theoretical models) and is, on the basis of the hybridization model, very likely rather small compared to the in-layer position. This gives a possible explanation for the large measured nonorienting fraction: It partly results from implanted ions that end up between the layers (with small QI) and is also due to lattice damage from the implantation, especially with the low-temperature implantations. Obviously this damage is (partly) annealed at room temperature.

It is important to mention that it is the sign of V_{zz} that makes the experimental and theoretical results comparable only for in-layer positions with neighboring vacancies.

Implantations of other isotopes in graphite mentioned in Table I yield various positions. From the angular dependence of the recoilless fractions, as observed in Mössbauer experiments, it was found that ^{133}Xe resides between the layers (its noble gas electronic configuration gives little opportunity for hybridization), and that two sites within the layers occur for ^{57}Co . The EFG that was measured in a nuclear-magnetic-resonance experiment on recoil-implanted ^{12}B nuclei could only be explained with the boron located at substitutional sites (position i1); two different quadrupole interactions were found for recoil-implanted ^{19}F in a time-differential perturbed-angular-correlation experiment, one of which corresponds to a nearly undisturbed F-C bond, also indicating a substitutional position.

It must be noted that there is yet little experience with calculations on molecular clusters of graphite-impurity systems. Particularly the choice of the atomic basis sets influences the occupation of the molecular orbitals and hence the calculated EFG. More details will be given in a forthcoming paper, where also results on B, F, Cs, and In will be considered. At this stage it can already be stated that the calculated QI of F and Cs in the reported lattice positions agree well with the experimental results, which supports this type of calculations. It is evident that the combination of experimental fitting and theoretical calculations has provided a reasonable picture of the origin of the EFG at impurities in HOPG.

The observed EFG is almost an order of magnitude larger than that of Hg implanted in noncubic metal hosts. This demonstrates the possibilities of using HOPG foils as a catcher material for detecting QI. The lower orienting fractions after the low-temperature implantation is a drawback in on-line NO experiments. However, in the cold implantations, the implanted dose was rather high, resulting perhaps in (partial) amorphization of the graphite. Improvements can be made and more experiments are needed to clarify this point.

ACKNOWLEDGMENTS

The coauthors at the Delft University of Technology would like to express their gratitude to the NICOLE and

ISOLDE collaborations at CERN for beam time and use of the implantation facility, respectively, and to H. C. Meijer and F. Mathu for their technical contributions and advice with regard to the dilution refrigerator. Dr. A. W. Moore from the Union Carbide Corporation is acknowledged for the supply of the HOPG. We thank the crew of the University of Bonn isotope separator for the ion implantations and other members of the University of

Bonn nuclear orientation group, especially D. Mayer and Miss I. Romanski, for help with the experiments. This work was supported financially by the Bundesministerium für Forschung und Technologie, Federal Republic of Germany, Contract No. 06BN181, and is also part of the research programme of the Foundation for Fundamental Research on Matter (FOM) financed through the Dutch Foundation for Pure Research (NWO).

*Present address: CERN, Division EPP, 1211 Geneva 23, Switzerland.

¹Y. Kuno, J. Imazato, K. Nishiyama, K. Nagamine, T. Yamazaki, K. Matsuta, S. Ise, Y. Nojiri, and T. Minamisono, *Hyperfine Interact.* **39**, 253 (1988).

²S. R. Dong, P. W. Martin, and J. G. Hooley, *Carbon* **22**, 453 (1984).

³S. R. Dong, S. El-Kateb, J. G. Hooley, and P. W. Martin, *Solid State Commun.* **45**, 791 (1983).

⁴S. R. Dong, J. G. Hooley, and P. W. Martin, *Hyperfine Interact.* **15-16**, 937 (1983).

⁵K. Bharuth-Ram, S. Connell, J. P. F. Sellschop, M. Stemmet, and H. Appel, *Radiat. Eff. Def. Solids* **108**, 73 (1989).

⁶L. E. Campbell, G. L. Montet, and G. J. Perlow, *Phys. Rev. B* **15**, 3318 (1977).

⁷M. de Potter and G. Langouche, *Phys. Lett.* **97A**, 404 (1983).

⁸P. W. Martin, S. R. Dong, and J. G. Hooley, *J. Chem. Phys.* **80**, 1677 (1984).

⁹P. W. Martin, S. R. Dong, and J. G. Hooley, *Phys. Rev. B* **33**, 4227 (1986).

¹⁰B. Kastelein, A. den Ouden, H. Postma, and H. C. Meijer, *Hyperfine Interact.* **35**, 89 (1987).

¹¹I. Dézsi, M. van Rossum, R. Coussement, G. Langouche, and S. R. Reintsema, *Hyperfine Interact.* **11** 255 (1981).

¹²J. M. Friedt, L. Soderholm, and R. Poinso, *Synth. Met.* **8**, 99 (1983).

¹³B. Kastelein, B. Borst, A. J. de Jong, H. Postma, and H. C. Meijer, *Hyperfine Interact.* **43**, 503 (1988).

¹⁴G. Kaindl, J. Feldhaus, U. Ladewig, and K. H. Frank, *Phys. Rev. Lett.* **50**, 123 (1983).

¹⁵B. Kastelein, H. Postma, L. Klostermann, J. K. W. M. Vemer, and H. C. Meijer, *Physica B* **165-166**, 921 (1990).

¹⁶W. N. Reynolds, *Physical Properties of Graphite* (Elsevier, New York, 1986).

¹⁷R. C. Tatar and S. Rabii, *Phys. Rev. B* **25**, 4126 (1982).

¹⁸D. Schroyen, M. Bruggeman, I. Dézsi, and G. Langouche, *Nucl. Instrum. Methods, Phys. Res. B* **15**, 341 (1986).

¹⁹B. T. Kelly, *Physics of Graphite* (Applied Science Publications, London, 1981).

²⁰M. R. Schmorak, *Nucl. Data Sheets*, **46**, 287 (1985).

²¹P. K. James, P. Herzog, and N. J. Stone, *Phys. Rev. B* **13**, 51 (1976).

²²G. Ulm, S. K. Bhattacharjee, P. Dabkiewicz, G. Huber, H.-J. Kluge, T. Kühl, H. Lochman, E.-W. Otten, and K. Wendt, *Z. Phys. A* **325**, 247 (1986).

²³P. Raghavan, *At. Data Nucl. Data Tables* **42**, 189 (1989).

²⁴R. M. Steffen and K. Alder, in *The Electromagnetic Interaction in Nuclear Spectroscopy*, edited by W. D. Hamilton

(North-Holland, Amsterdam, 1975), Chap. 12, p. 505.

²⁵K. S. Krane, in *Low-Temperature Nuclear Orientation*, edited by N. J. Stone and H. Postma (North-Holland, Amsterdam, 1986), Chap. 2.

²⁶B. G. Turrell, in *Low-Temperature Nuclear Orientation* (Ref. 25), Chap. 10.

²⁷M. G. Clark, in *Molecular Structure and Properties*, edited by A. D. Buckingham, Vol. 2 of *Physical Chemistry, Series 2* (Butterworths, London, 1975), Chap. 7.

²⁸E. N. Kaufmann and R. J. Vianden, *Rev. Mod. Phys.* **51**, 161 (1979).

²⁹N. W. Ashcroft and N. D. Mermin, *Solid State Physics* (Holt, Rinehart, and Winston, New York, 1976).

³⁰E. Kaxiras and K. C. Pandey, *Phys. Rev. Lett.* **61**, 2693 (1988).

³¹F. D. Feiock and W. R. Johnson, *Phys. Rev.* **187**, 39 (1969).

³²A. Dalgarno and H. A. J. McIntyre, *Proc. Phys. Soc.* **85**, 47 (1965).

³³A. A. Gusev, *Fiz. Tekh. Poluprovodn.* **21**, 1332 (1987) [*Sov. Phys. Semicond.* **21**, 810 (1987)].

³⁴M. J. Frisch, M. Head-Gordon, G. W. Trucks, J. B. Foresman, H. B. Schlegel, K. Raghavachari, M. Robb, J. S. Binkley, C. Gonzales, D. J. Defrees, D. J. Fox, R. A. Whiteside, R. Seeger, C. F. Melius, J. Baker, R. L. Martin, L. R. Kahn, J. J. P. Stewart, S. Topiol and J. A. Pople, *Gaussian 90 Revision F* (Gaussian Inc., Pittsburgh PA, 1990).

³⁵J. Sauer, *Chem. Rev.* **89**, 199 (1989).

³⁶*Handbook of Gaussian Basis Sets*, edited by S. Huzinaga (Elsevier, Amsterdam, 1985).

³⁷*Methods of Electronic Structure Theory*, edited by H. F. Schaefer III (Plenum, New York, 1977).

³⁸P. Herzog, K. Krien, J. C. Soares, H.-R. Folle, K. Freitag, F. Reuschenbach, M. Reuschenbach, and R. Trzcinski, *Phys. Lett.* **66A**, 495 (1978).

³⁹I. Berkes, G. Marest, J. Sau, H. Sayouty, P. Put, R. Coussement, and G. Scheveneels, *Hyperfine Interact.* **15-16**, 233 (1983).

⁴⁰J. C. Soares, K. Krien, P. Herzog, H.-R. Folle, K. Freitag, F. Reuschenbach, M. Reuschenbach, and R. Trzcinski, *Z. Phys. B* **31**, 395 (1978).

⁴¹J. Lindhard, M. Scharff, and H. E. Schiøtt, *K. Dan. Vidensk. Selsk. Mat. Fys. Medd.* **33**, 1 (1963).

⁴²B. Kastelein, H. Postma, R. D. van Bergen, and H. C. Meijer (unpublished).

⁴³B. Kastelein, J. K. W. M. Vemer, H. J. van der Morel, and H. Postma, *Nucl. Methods Phys. Res. A* **316**, 158 (1992).

⁴⁴B. Kastelein, H. J. van der Marel, J. Andriessen, H. Postma, and F. Pleiter (unpublished).